



# Controllable molecular configuration for significant improvement of blue OLEDs based on novel twisted anthracene derivatives



Juan Wang<sup>a,b</sup>, Xia Lou<sup>c</sup>, Yaqing Liu<sup>b</sup>, Guizhe Zhao<sup>b</sup>, Amjad Islam<sup>a</sup>, Suidong Wang<sup>c,\*</sup>, Ziyi Ge<sup>a,\*</sup>

<sup>a</sup> Ningbo Key Laboratory of Silicon and Organic Thin Film Optoelectronic Technologies, Ningbo Institute of Materials Technology & Engineering, Chinese Academy of Sciences, Ningbo 315201, PR China

<sup>b</sup> Institute of Materials Science & Engineering, The North University of China, Taiyuan 030051, PR China

<sup>c</sup> Institute of Functional Nano & Soft Materials, Soochow University, Suzhou 215123, PR China

## ARTICLE INFO

### Article history:

Received 15 December 2014

Received in revised form

3 February 2015

Accepted 4 March 2015

Available online 12 March 2015

### Keywords:

Blue emission

Twisted anthracene derivatives

Molecular configuration

OLEDs

Significant improvement

Fluorescent emitters

## ABSTRACT

Two novel twisted anthracene derivatives, 2-(4-(10-(phenanthren-9-yl)anthracen-9-yl)phenyl)-1-phenyl-1H-phenanthro[9,10-d]imidazole (p-PABPI) and 2-(3-(10-(phenanthren-9-yl)anthracen-9-yl)phenyl)-1-phenyl-1H-phenanthro-[9,10-d]imidazole (m-PABPI), have been synthesized. Their photo-physical and photochemical properties are also investigated systemically. The non-doped fluorescent organic light-emitting diodes are fabricated by using anthracene derivatives as the emitters. The maximum current efficiencies are achieved to be 3.98 and 1.32 cd A<sup>-1</sup> and the maximum power efficiencies are 2.80 and 1.14 lm W<sup>-1</sup>, respectively. The external quantum efficiency maximum (EQE<sub>max</sub>) is 3.61% and 1.33% for p-PABPI and m-PABPI. Intriguingly, the efficiencies of p-PABPI are almost three times larger than that of m-PABPI with only the different molecular configuration. The results revealed a new rule of molecular design based on anthracene derivatives for obtaining high performance blue emission materials.

© 2015 Elsevier Ltd. All rights reserved.

## 1. Introduction

Organic light-emitting diodes (OLEDs) have been attracting great scientific and industrial attention due to their potential applications in high-quality flat-panel displays and solid-state lighting [1–3]. For full-color display, red (R), green (G), and blue (B) emission of relatively equal stability, efficiency, and color purity is immensely required. Among the color of RGB, the blue emitter is of special significance because such emitters not only effectively reduce the power consumption, but can also be utilized to generate light of other colors by energy cascade to a lower-energy fluorescent or phosphorescent dopants [4]. However, owing to their intrinsic band gap, the state of art performance of blue OLEDs is inferior to that of green and red [4–6]. Therefore, blue OLEDs with high efficiency have been urgently required to kick off the commercialization of OLEDs.

Recently, great efforts have been made to devise efficient blue phosphors due to their advantage of harvesting both singlet and

triplet excitons, and EQE<sub>max</sub> of blue electrophosphorescence reported over 20% [7–10]. However, blue phosphorescent emitters are less preferable than their fluorescent counterparts because of the difficulties encountered in the synthesis of large band-gap dopants and poor color purity, stability, longevity and expensive price [11]. Hence, design and synthesis of highly efficient blue fluorescent emitters is still a key requirement to accelerate the industrialization of OLEDs.

Since the first report about organic electroluminescence from organic crystals of anthracene was observed in the 1960s [12], there has been great interest in the study of anthracene derivatives as an attractive building block for OLEDs. However, anthracene with its intrinsic planarity and grid structure easily causes fluorescence concentration quenching and emission wavelength bathochromic shift in the solid state. In this regard, Adachi et al. reported one of the anthracene derivatives (DPA) by introducing two phenyl units at 9,10-positions of anthracene and achieved a luminescence of 0.09 cd m<sup>-2</sup> at 100 mA cm<sup>-2</sup> [13]. However, the reported DPA showed easy crystallization in the solid-state thin film, which would directly lead to low device efficiency. Then, Lee et al. designed 2-methyl-9,10-di(2-naphthyl)anthracene based on the

\* Corresponding authors.

E-mail addresses: [wangsd@suda.edu.cn](mailto:wangsd@suda.edu.cn) (S. Wang), [geziyi@nimte.ac.cn](mailto:geziyi@nimte.ac.cn) (Z. Ge).

structure of DPA, and the electroluminescent devices with styrylamine as dopant were fabricated, and the efficiencies of  $9.7 \text{ cd A}^{-1}$  and  $5.5 \text{ lm W}^{-1}$  at  $20 \text{ mA cm}^{-2}$  were achieved. It means the crystallization in the film can be efficaciously suppressed [14]. Prior to the symmetrical structure, the unsymmetrical structure can be a promising candidate for the formation of efficient, stable and amorphous film. For example, Tian et al. reported an unsymmetrical anthracene derivative with triphenylamine and imidazole, the non-doped device showed a maximum current efficiency of  $3.33 \text{ cd A}^{-1}$  [15]. Subsequently, Zhuang et al. designed and synthesized three novel blue-emitters with unsymmetrical structure by introducing 9-(naphthalen-2-yl)anthracene or pyrene, and gained a maximum current efficiency of  $4.99 \text{ cd A}^{-1}$  with  $\text{CIE}_{x,y}$  (0.15, 0.17) for the non-doped OLED devices [16]. Recently, Liu et al. reported two twisted anthracene derivatives and showed high efficiency deep-blue emission [17]. Notably, the singlet generation fraction is more than 25% by using 10,10'-(Bis-9-pentylcarbazol-3-yl)-[9,9']-bianthryl (CzBACz) as emitter. In view of this, it is highly desirable to develop novel materials with twisted D-A structure to achieve high efficiency. Some progress has been made to obtain high efficiency by synthesizing some materials with twisted donor-acceptor (D-A) structures [18,19]. Therefore, the research about twisted anthracene derivatives is still of significant importance to the development of the blue OLEDs.

Herein, we report synthesis and characterization of two novel twisted anthracene derivatives isomers, 2-(4-(10-(phenanthren-9-yl)anthracen-9-yl)phenyl)-1-phenyl-1H-phenanthro[9,10-d]imidazole (p-PABPI) and 2-(3-(10-(phenanthren-9-yl)anthracen-9-yl)phenyl)-1-phenyl-1H-phenanthro[9,10-d]imidazole (m-PABPI). It is particularly interesting to compare the electroluminescent properties of p-PABPI and m-PABPI, both have the same constructed unit. When the molecular configuration of these derivatives is changed, their EL devices are exhibited similar blue emission but electroluminescent efficiency is varied almost three times.

## 2. Experimental

### 2.1. Materials and measurements

Fourier transform-infrared (FTIR) spectra were performed using Thermo Nicolet 6700 spectrophotometer. Nuclear magnetic resonance ( $^1\text{H}$  NMR &  $^{13}\text{C}$  NMR) spectra were recorded on a Bruker DRX-400 spectrometer with chemical shifts. ESI-MS spectra were measured with a FINNIGAN Trace DSQ mass spectrometer at 70 eV. Elemental analyses were performed with a PerkinElmer 2400 II elemental analyzer. UV-vis absorption spectra were recorded on a Perkin-Elmer Lambda 950 spectrophotometer. Photoluminescent (PL) measurements were with a FLS920 spectrophotometer in a solution of  $10^{-6}$  mol/L and a solid state, respectively. Thermogravimetric analyses (TGA) were carried out using a PerkinElmer Pyris thermogravimeter at  $10^\circ\text{C min}^{-1}$  under nitrogen flushing. Cyclic voltammetry (CV) measurements were performed on a CHI 660D electrochemical workstation with a Pt disk as the working electrode, a Pt wire as the counter electrode, and Ag/AgCl as the reference electrode, in a dichloromethane solution containing 0.1 M of tetrabutylammonium hexafluorophosphate as the supporting electrolyte.

### 2.2. Synthesis of the compounds

9,10-dibromoanthracene, (4-formylphenyl)boronic acid, (3-formylphenyl)boronic acid, 9-phenanthreneboronic acid, 9,10-phenanthraquinone, aniline were purchased from TCI co.

#### 2.2.1. Preparation of 4-(10-bromoanthracen-9-yl)benzaldehyde (1)

In a 500 mL round-bottomed flask charged with nitrogen, 9,10-dibromoanthracene (9.21 g, 18 mmol), (4-formylphenyl)boronic acid (1.35 g, 9 mmol) and bis(triphenyl phosphine)palladium(II) chloride (0.31 g, 0.9 mmol) were dissolved in THF (100 mL) and stirred for 10 min. A solution of 10 mL potassium carbonate (2 M) was added and the reaction mixture was heated to  $70^\circ\text{C}$  for 12 h. The reaction mixture was cooled to room temperature and extracted with dichloromethane and water. The organic layer was evaporated with a rotary evaporator. The crude product was purified by column chromatography to give a yellow powder. Yield: 1.65 g, 51%.  $^1\text{H}$  NMR (400 MHz,  $\text{CDCl}_3$ )  $\delta$  10.20 (s, 1H), 8.56–8.65 (m, 1H), 8.09 (dd, 3H,  $J_1 = 7.92 \text{ Hz}$ ,  $J_2 = 8.39 \text{ Hz}$ ), 7.54–7.64 (m, 4H), 7.48 (t, 2H,  $J = 7.45 \text{ Hz}$ ), 7.38 (dd, 2H,  $J_1 = 10.92 \text{ Hz}$ ,  $J_2 = 7.76 \text{ Hz}$ ), which was consistent with the reported literature [20].

#### 2.2.2. Preparation of 3-(10-bromoanthracen-9-yl)benzaldehyde (2)

Using the same procedure described for (1), 3-(10-bromoanthracen-9-yl)benzaldehyde was synthesized. Yield: 1.77 g, 54.6%.  $^1\text{H}$  NMR (400 MHz,  $\text{CDCl}_3$ )  $\delta$  10.10 (s, 1H), 8.61 (d, 2H,  $J = 8.94 \text{ Hz}$ ), 8.07 (d, 1H,  $J = 7.57 \text{ Hz}$ ), 7.91 (s, 1H), 7.75 (t, 1H,  $J = 7.70 \text{ Hz}$ ), 7.66 (d, 1H,  $J = 7.55 \text{ Hz}$ ), 7.58 (t, 2H,  $J = 7.70 \text{ Hz}$ ), 7.52 (d, 2H,  $J = 8.83 \text{ Hz}$ ), 7.37 (t, 2H,  $J = 7.49 \text{ Hz}$ ), which was consistent with the reported literature [21].

#### 2.2.3. Preparation of 4-(10-(phenanthren-9-yl)anthracen-9-yl)benzaldehyde (3)

In a three necked flask filled with nitrogen, 4-(10-bromoanthracen-9-yl)benzaldehyde (1.44 g, 4 mmol), 9-phenanthreneboronic acid (1.11 g, 5 mmol) and bis(triphenyl phosphine)palladium(II)chloride (0.14 g, 0.2 mmol) were dissolved in THF (30 mL), forming yellow solution. A solution of 10 mL potassium carbonate (2 M) was added and the reaction mixture was heated to  $70^\circ\text{C}$  for 10 h. After that, the reaction mixture was cooled to room temperature and extracted with dichloromethane and water for three times. The organic layer was evaporated with a rotary evaporator. The crude product was purified by column chromatography to give a yellow powder. Yield: 1.10 g, 60%.  $^1\text{H}$  NMR (400 MHz,  $\text{CDCl}_3$ )  $\delta$  10.25 (s, 1H), 8.89 (dd, 2H,  $J_1 = 4.23 \text{ Hz}$ ,  $J_2 = 3.83 \text{ Hz}$ ), 8.19 (t, 2H,  $J = 6.16 \text{ Hz}$ ), 7.94 (d, 1H,  $J = 7.58 \text{ Hz}$ ), 7.88 (s, 1H), 7.80 (d, 2H,  $J = 7.58 \text{ Hz}$ ), 7.76 (dd, 2H,  $J_1 = 6.45 \text{ Hz}$ ,  $J_2 = 8.27 \text{ Hz}$ ), 7.68 (t, 4H,  $J = 7.90 \text{ Hz}$ ), 7.62 (d, 2H,  $J = 8.85 \text{ Hz}$ ), 7.38–7.33 (m, 3H), 7.24 (t, 2H,  $J = 7.58 \text{ Hz}$ ); ESI-MS ( $m/z$ ): 459.2 ( $\text{M}^+ + \text{H}$ ).

#### 2.2.4. Preparation of 3-(10-(phenanthren-9-yl)anthracen-9-yl)benzaldehyde (4)

3-(10-(phenanthren-9-yl)anthracen-9-yl)benzaldehyde was obtained with the same procedure described for (3). Yield: 1.12 g, 61%.  $^1\text{H}$  NMR (400 MHz,  $\text{CDCl}_3$ )  $\delta$  10.20 (d, 1H,  $J = 4.99 \text{ Hz}$ ), 8.90 (dd, 2H,  $J_1 = 3.57 \text{ Hz}$ ,  $J_2 = 3.69 \text{ Hz}$ ), 8.16–8.14 (m, 2H), 7.95 (dd, 1H,  $J_1 = 4.04 \text{ Hz}$ ,  $J_2 = 3.95 \text{ Hz}$ ), 7.91–7.84 (m, 3H), 7.79 (t, 1H,  $J = 7.62 \text{ Hz}$ ), 7.69 (dd, 4H,  $J_1 = 7.90 \text{ Hz}$ ,  $J_2 = 8.64 \text{ Hz}$ ), 7.63 (d, 2H,  $J = 8.87 \text{ Hz}$ ), 7.36 (t, 3H,  $J = 7.75 \text{ Hz}$ ), 7.26 (t, 3H,  $J = 4.25 \text{ Hz}$ ); ESI-MS ( $m/z$ ): 458.1 ( $\text{M}^+$ ).

#### 2.2.5. Synthesis of 2-(4-(10-(phenanthren-9-yl)anthracen-9-yl)phenyl)-1-phenyl-1H-phenanthro[9,10-d]imidazole (p-PABPI)

4-(10-(phenanthren-9-yl)anthracen-9-yl)benzaldehyde (0.92 g, 2 mmol), 9,10-phenanthraquinone (0.62 g, 3 mmol) and ammonium acetate (0.3 g, 5 mmol) were dissolved in acetic acid (30 mL). The reaction mixture was stirred in a three-necked flask for 30 min. Then, aniline (0.46 g, 5 mmol) was added to the mixture and refluxed overnight at  $120^\circ\text{C}$ . After cooled to room temperature, the reaction mixture was poured into much water, forming a large quantity of precipitates. The solid was collected by filtration and

dissolved in dichloromethane. The mixed organic layer was evaporated with a rotary evaporator. The crude product was purified by column chromatography to give a yellow target product. Yield: 1.20 g, 83.2%. FTIR (KBr,  $\text{cm}^{-1}$ ) 3060, 756, 725 (aromatic C–H), 1596, 1496, 1450, 1439 (aromatic C=C), 1474 (C=N), 1345 (C–N).  $^1\text{H}$  NMR (400 MHz,  $\text{CDCl}_3$ )  $\delta$  9.01 (d, 1H,  $J = 7.99$  Hz), 8.90 (d, 2H,  $J = 8.16$  Hz), 8.84 (d, 1H,  $J = 8.50$  Hz), 8.78 (d, 1H,  $J = 8.67$  Hz), 7.94 (t, 2H,  $J = 7.99$  Hz), 7.89 (s, 2H), 7.81 (d, 2H,  $J = 7.65$  Hz), 7.76–7.67 (m, 10H), 7.59 (dd, 4H,  $J_1 = 8.69$  Hz,  $J_2 = 7.90$  Hz), 7.51 (d, 1H,  $J = 8.10$  Hz), 7.38–7.31 (m, 5H), 7.24 (t, 3H,  $J = 7.11$  Hz).  $^{13}\text{C}$  NMR (100 MHz,  $\text{CDCl}_3$ )  $\delta$  135.27, 132.68, 131.73, 131.56, 130.66, 130.51, 130.44, 129.99, 129.76, 129.68, 129.18, 128.79, 128.56, 127.69, 127.49, 127.14, 126.99, 126.95, 126.92, 126.84, 126.73, 126.55, 125.34, 124.26, 123.17, 122.88, 122.75, 121.00; ESI-MS ( $m/z$ ): 723.3 ( $\text{M}^+ + \text{H}$ ); Anal. calcd for  $\text{C}_{55}\text{H}_{34}\text{N}_2$ : C, 91.38; H, 4.74; N, 3.88; Found: C, 91.41; H, 4.71; N, 3.85.

#### 2.2.6. Synthesis of 2-(3-(10-(phenanthren-9-yl)anthracen-9-yl)phenyl)-1-phenyl-1H-phenanthro[9,10-d]imidazole (m-PABPI)

Using the same procedure described for p-PABPI, 2-(3-(10-(phenanthren-9-yl)anthracen-9-yl)phenyl)-1-phenyl-1H-phenanthro[9,10-d]imidazole (m-PABPI) was obtained. Yield: 1.17 g, 81%. FTIR (KBr,  $\text{cm}^{-1}$ ) 3057, 754, 725, (aromatic C–H), 1597, 1496, 1451, 1438 (aromatic C=C), 1476 (C=N), 1346 (C–N).  $^1\text{H}$  NMR (400 MHz,  $\text{CDCl}_3$ )  $\delta$  8.94 (d, 1H,  $J = 6.32$  Hz), 9.90 (d, 2H,  $J = 8.10$  Hz), 8.80 (d, 1H,  $J = 8.49$  Hz), 8.74 (d, 1H,  $J = 8.49$  Hz), 7.98 (dd, 2H,  $J_1 = 7.11$  Hz,  $J_2 = 7.30$  Hz), 7.89 (d, 1H,  $J = 8.10$  Hz), 7.82–7.75 (m, 3H), 7.73–7.63 (m, 5H), 7.59–7.48 (m, 11H), 7.37 (dd, 1H,  $J_1 = 7.74$  Hz,  $J_2 = 7.26$  Hz), 7.30 (m, 2H), 7.24 (q, 4H,  $J = 7.50$  Hz).  $^{13}\text{C}$  NMR (100 MHz,  $\text{CDCl}_3$ )  $\delta$  139.28, 135.38, 135.23, 135.19, 132.65, 132.62, 132.22, 131.72, 131.68, 130.64, 130.55, 130.51, 130.45, 130.41, 130.05, 129.92, 129.84, 129.82, 129.40, 128.79, 128.73, 127.45, 127.01, 126.80, 125.52, 125.31, 124.35, 123.12, 122.87, 122.77, 121.01; ESI-MS ( $m/z$ ): 722.1 ( $\text{M}^+$ ); Anal. calcd for  $\text{C}_{55}\text{H}_{34}\text{N}_2$ : C, 91.38; H, 4.74; N, 3.88; Found: C, 91.37; H, 4.70; N, 3.93.

### 2.3. Device fabrication and characterization

Before the fabrication of OLEDs, the compounds p-PABPI and m-PABPI were purified by vacuum sublimation with the first pipe heating up to 360 °C. The ITO-coated glass substrates were routinely cleaned and then treated with UV-ozone for 15 min. Two kinds of devices were constructed with the structure of ITO/MoO<sub>3</sub> (5 nm)/NPB (40 nm)/TCTA (5 nm)/p-PABPI or m-PABPI (20 nm)/B<sub>3</sub>PyPB (40 nm)/LiF (1 nm)/Al (100 nm) and ITO/MoO<sub>3</sub> (5 nm)/NPB (40 nm)/TCTA (5 nm)/p-PABPI or m-PABPI: CBP (20 nm, 3 wt% or 6 wt%)/B<sub>3</sub>PyPB (40 nm)/LiF (1 nm)/Al (100 nm). All the organic and inorganic layers were manufactured in sequence at 10<sup>-6</sup> Torr. The deposition rate of organic compounds was 0.9–1.1 Å s<sup>-1</sup>. The electroluminescence spectra and the Commission Internationale de l'Eclairage coordination of the device were tested on a PR655 spectra scan spectrometer. The luminance–current and density–voltage characteristics were measured simultaneously from the measurement of the EL spectra by combining the spectrometer with a Keithley 2400 programmable voltage–current source. All measurements were conducted at room ambient conditions.

## 3. Results and discussion

### 3.1. Synthesis

Scheme 1 displays the synthetic route of the molecules, which contain an anthracene-phenanthrene and imidazole unit. Our design of the anthracene-type compounds was inspired by the twisted structure of anthracene derivatives, a widely used material

for fluorescent OLEDs that exhibits a good blue emission [18,19]. To expand the family of twisted anthracene-type derivative with excellent performance of OLEDs, we adopted anthracene and its derivatives as the plane to form twisted structure. In addition, recently we have reported one kind of the constitution isomerism to manage their excited-state and intramolecular charge-transfer [22,23]. Therefore, based on our group's work, two novel twisted anthracene derivatives were designed with the same building blocks but only difference of phenyl substitution position. As shown in Scheme 1, the compounds **1**, **2**, **3** and **4** were prepared by the Suzuki coupling with high yields. Subsequently, the target compounds were obtained by condensing **3** and **4** with 9,10-phenanthraquinone, and aniline (more than 80% yield). All the compounds were characterized by  $^1\text{H}$  and  $^{13}\text{C}$  NMR spectrometry, mass spectrometry, and elemental analysis.

### 3.2. Thermal properties

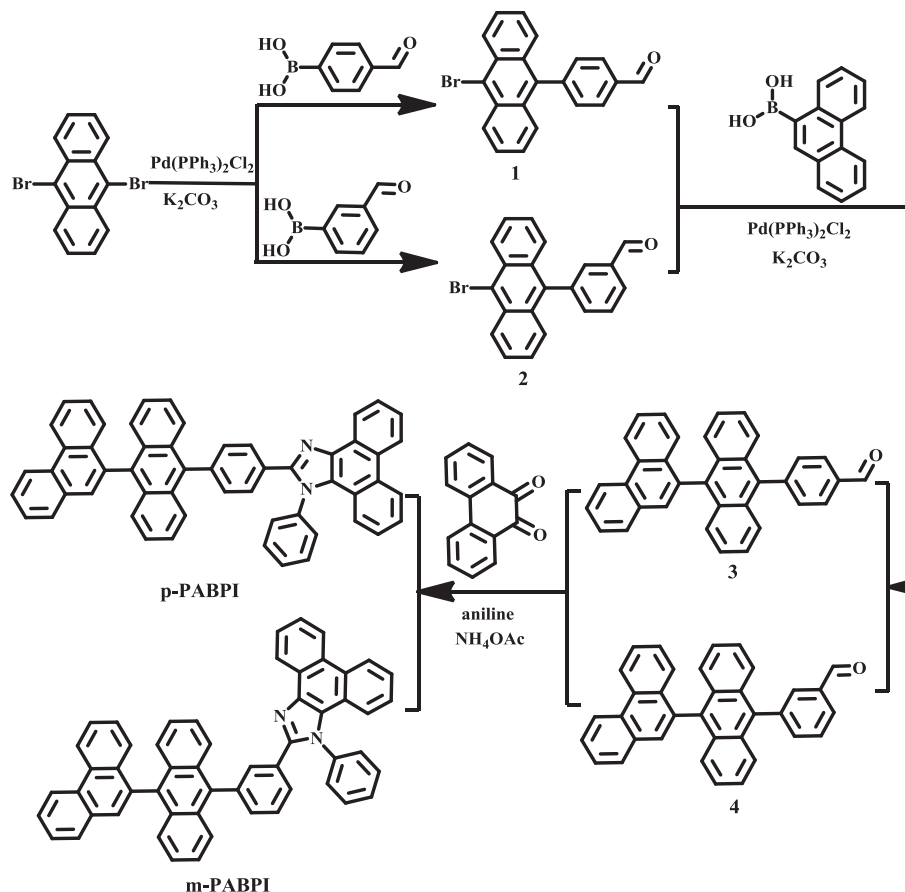
The thermal properties of p-PABPI and m-PABPI were measured using thermogravimetric analysis (TGA) under a nitrogen atmosphere, and their related data are illustrated in Table 1 and Fig. 1. As shown in Fig. 1, p-PABPI and m-PABPI exhibit high decomposition temperature ( $T_d$ , 5% weight loss), which are 511 and 438 °C, respectively. The high  $T_d$  values allow to use these derivatives in the fabrication of high performance OLEDs through vacuum thermal evaporation technology.

### 3.3. Theoretical calculations

The ground-state geometries and the frontier molecular orbital energy levels were calculated using density functional theory (DFT) in Gaussian 03 program. From Fig. 2, the calculated highest occupied molecular orbital (HOMO) and lowest unoccupied molecular orbital (LUMO) of p-PABPI and m-PABPI are found to be mainly localized on the anthracene moiety. The 9,10-substituents are leaned almost 90° to the anthracene core due to large torsional stress. Both compounds with twisted structure can efficiently prevent molecular recrystallization and excimer or exciplex formation [24]. The HOMO and LUMO energy levels of p-PABPI are calculated to be –5.11 and –2.66 eV, and the HOMO and LUMO energy levels of m-PABPI are –5.07 eV and –2.60 eV, respectively.

### 3.4. Photophysical and electrochemical properties

The UV–vis absorption and photoluminescent (PL) spectra of p-PABPI and m-PABPI in dilute  $\text{CH}_2\text{Cl}_2$  solutions as well as in the solid film are shown in Fig. 3. A summary of the precise photophysical data of the compounds is also given in Table 1. The p-PABPI and m-PABPI exhibited similar absorption spectra (360, 377 and 397 nm for p-PABPI, 357, 375 and 396 nm for m-PABPI) in the dilute solution, which can be originated from the  $\pi$ – $\pi^*$  transition of the isolated anthracene core with archetypal vibronic characteristics [25]. In the film state, they exhibited a 3–5 nm bathochromic-shift. Compared with UV–vis absorption spectra, fluorescence spectra of p-PABPI and m-PABPI in  $\text{CH}_2\text{Cl}_2$  showed maximum emission wavelengths at 434 and 413 nm. Also, the shape of the spectrum in film and solution was rather similar, but there was an about 14 nm red-shifted in thin films. Furthermore, it is highly worth noting that the PL spectrum of p-PABPI exhibits more red-shifted as compared to m-PABPI. It can be assigned to the greater steric hindrance of m-PABPI, which leads to an increase in non-planarity and prevents close molecular stacking in the solid film [26]. The fluorescent quantum yields ( $\Phi_F$ ) of them are 74% (p-PABPI) and 56% (m-PABPI), respectively, indicating both are promising candidates for blue emitters in OLEDs. Obviously, the fluorescent quantum yields ( $\Phi_F$ )



**Scheme 1.** The synthetic route to p-PABPI, m-PABPI.

of p-PABPI is higher than that of m-PABPI. It can be attributed to the largely twisted structure of m-PABPI, which will reduce the conjugation and suppress its fluorescence [27].

The HOMO energy levels of p-PABPI and m-PABPI were measured by cyclic voltammetry (CV), and the results are shown in Fig. 4 and Table 1. The onset oxidation peaks ( $E_{\text{ox}}$ ) of p-PABPI and m-PABPI are 1.09 and 0.97 eV versus the ferrocenium/ferrocene redox couple, respectively. HOMO values are calculated from the formula of  $E_{\text{HOMO}} = -([E_{\text{onset}}]_{\text{ox}} + 4.4)$ . The values of p-PABPI and m-PABPI are  $-5.59$  and  $-5.37$  eV, respectively. Such deep HOMO energy levels are lower than the work function of ITO, which can effectively reduce the energy barrier for hole injection into the emission layer and improve the device efficiency [28]. The energy band gaps ( $E_g$ ) of

p-PABPI and m-PABPI are calculated to be about 2.94 and 2.98 eV, which are determined from the threshold of UV–vis absorption spectra. Finally, the LUMO levels of p-PABPI and m-PABPI are found to be  $-2.65$  and  $-2.39$  eV.

### 3.5. Electroluminescent properties

Initially, to evaluate electroluminescent (EL) performances of p-PABPI and m-PABPI, the non-doped OLEDs with the structure of

**Table 1**  
Thermal properties, optional properties and energy levels of p-PABPI and m-PABPI.

Compounds	$T_d$ (°C)	$\lambda_{\text{maxAbs}}^{a,b}$ (nm)	$\lambda_{\text{maxPL}}^{a,b}$ (nm)	HOMO/LUMO <sup>exp</sup> ( $E_g^{\text{opt}}$ ) <sup>c</sup> (eV)	HOMO/LUMO <sup>cal</sup> ( $E_g^{\text{opt}}$ ) <sup>d</sup> (eV)
p-PABPI	511	360, 377,	434.2	$-5.59/-2.65(2.94)$	$-5.11/-2.66(2.45)$
		397			
		364, 380,	448.4		
		401			
m-PABPI	438	357, 375,	413.0	$-5.37/-2.39(2.98)$	$-5.07/-2.60(2.47)$
		396			
		362, 378,	426.6		
		401			

<sup>a</sup> Measured in  $\text{CH}_2\text{Cl}_2$ .

<sup>b</sup> Measured in solid film on quartz plates.

<sup>c</sup> Estimated based on absorption onset and cyclic-voltammetry.

$E_{\text{HOMO}} = -(qE_{\text{ox}} + 4.4)$  eV,  $E_{\text{LUMO}} = E_g^{\text{opt}} + E_{\text{HOMO}}$ .

<sup>d</sup> DFT calculation with B3LYP/6-31G.

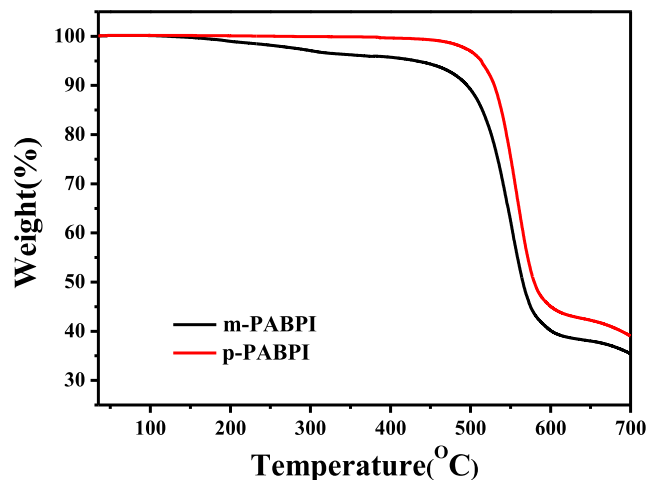


**Fig. 1.** TGA thermograms of p-PABPI and m-PABPI recorded at a heating rate of  $10^\circ\text{C min}^{-1}$ .

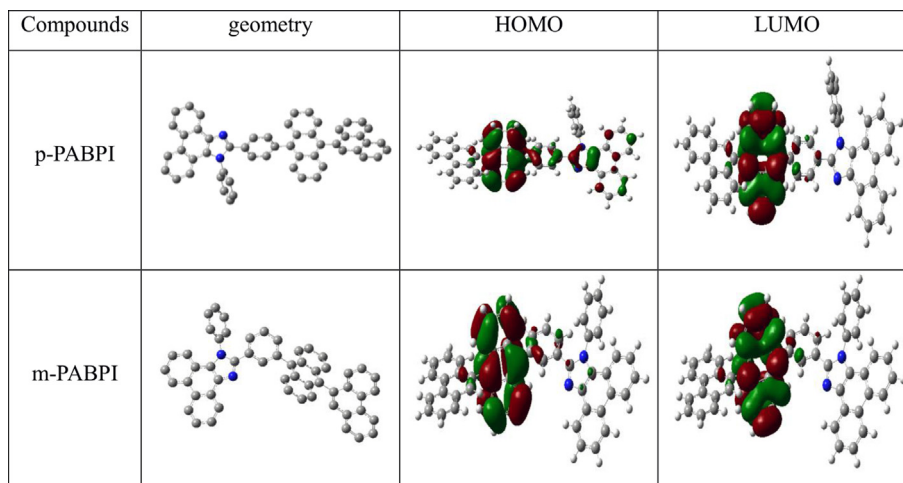


Fig. 2. Molecular orbital distribution and optimized geometries of p-PABPI and m-PABPI.

ITO/MoO<sub>3</sub> (5 nm)/NPB (40 nm)/TCTA (5 nm)/EML: p-PABPI and m-PABPI (20 nm)/B<sub>3</sub>PyPB (40 nm)/LiF (1 nm)/Al (100 nm) were fabricated by vacuum deposition. Indium tin oxide (ITO) and Al were utilized as anode and cathode, MoO<sub>3</sub> was used as a hole injecting layer, N,N'-bis(naphthalene-1-yl)-N,N'-bis(phenyl)-benzidine (NPB) was as a hole transporting layer, 4,4',4''-tri(N-carbazolyl)benzene (TCTA) was as an electron blocking layer, 3,3'',5,5''-tetra-(pyridin-3-yl)-1,1':3',1''-terphenyl (B<sub>3</sub>PyPB) as an electron transporting and hole blocking layer, and LiF was used as an electron injecting layer.

A and B represent the non-doped devices based on p-PABPI and m-PABPI as emitters. Performance of the devices is shown in Table 2 and Fig. 5. From Fig. 5a, the maximum emission ( $\lambda_{\max}$ ) of p-PABPI and m-PABPI are located at 456 and 448 nm, and the full width at half-maximum (FWHM) values are located at 59 and 60 nm, respectively. There is a little red-shift for both, relative to photoluminescent (PL) spectra, which can be attributed to face-to-face  $\pi$ - $\pi$  stacking for the vacuum-deposited film [29]. The current density-voltage-luminance characteristics of the devices are given in Fig. 5b. Maximum luminance of p-PABPI-based OLEDs are as high as 18,980 cd m<sup>-2</sup>, but the devices based on m-PABPI are only 6140 cd m<sup>-2</sup>. As shown in Fig. 5c, the maximum current efficiency for p-PABPI and m-PABPI is 3.98 and 1.32 cd A<sup>-1</sup>, and the maximum power efficiency is 2.80 and 1.14 lm W<sup>-1</sup>, respectively. The EQE<sub>max</sub> of the non-doped fluorescent OLEDs are 3.61% for p-PABPI and

1.33% for m-PABPI from Fig. 5d. Notably, when substituted position of phenyl is changed between anthracene and imidazole for p-PABPI and m-PABPI, the efficiency is changed by approximately three times, which results from the higher PL quantum yields of p-PABPI and the significantly improved carrier injection/transport ability of p-PABPI (Fig. S9) [30]. Interestingly, when luminance is up to 1000 cd m<sup>-2</sup>, the current efficiency for p-PABPI-based devices still maintain an upward trend. Likewise, the results illustrate that p-PABPI has much lower roll-off. The CIE coordinates (x, y) of p-PABPI- and m-PABPI-based devices are discovered to be (0.15, 0.13) and (0.16, 0.12) from Table 2, which is classified as strong blue emission. Overall, the non-doped devices based on p-PABPI as an emitter are superior than m-PABPI-based devices.

Then, to further discuss the potential application of the compounds, the doped OLED devices with the configuration of ITO/MoO<sub>3</sub> (5 nm)/NPB (40 nm)/TCTA (5 nm)/p-PABPI or m-PABPI: CBP (20 nm, 3 wt% or 6 wt%)/B<sub>3</sub>PyPB (40 nm)/LiF (1 nm)/Al (100 nm) were fabricated by vacuum deposition, where CBP was used as a host. In Table 2, The devices p1 and p2 represent 3% and 6% dopant concentration for p-PABPI as the emitting dopant, and the devices m1 and m2 stand for 3% and 6% dopant concentration for m-PABPI as the emitting dopant [31].

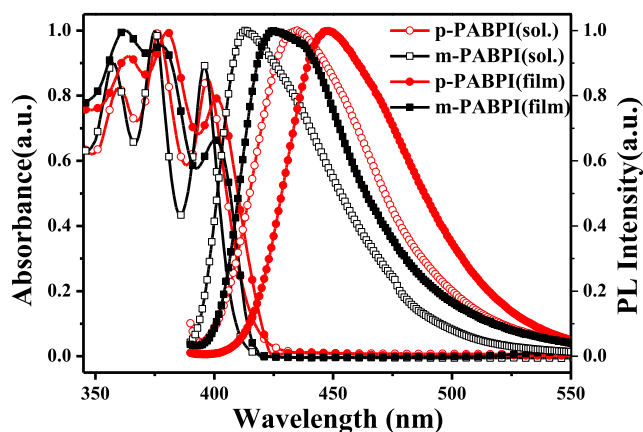


Fig. 3. UV absorption and PL spectra of p-PABPI and m-PABPI.

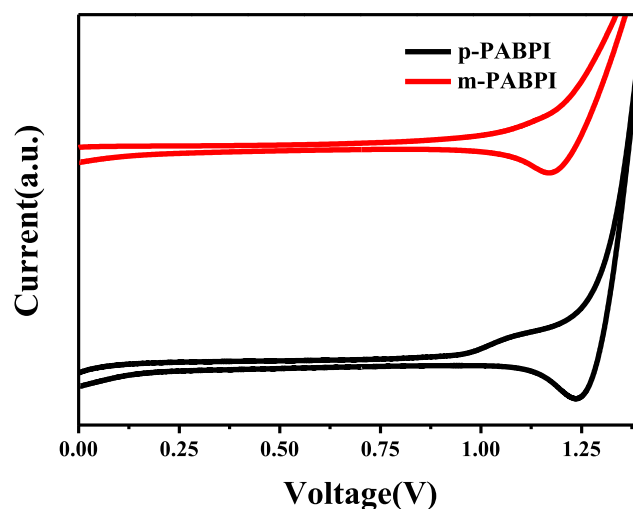


Fig. 4. Cyclic voltammograms of compounds p-PABPI and m-PABPI in CH<sub>2</sub>Cl<sub>2</sub>.

**Table 2**  
Electroluminescent data of the devices.

Device	CIE <sup>a</sup> (x,y)	I <sub>max</sub> (cd m <sup>-2</sup> )	λ <sub>max</sub> EL <sup>a</sup> (nm)	FWHM <sup>a</sup> (nm)	CE <sub>max</sub> <sup>b,c</sup> (cd A <sup>-1</sup> )	PE <sub>max</sub> <sup>b,c</sup> (lm W <sup>-1</sup> )	EQE <sub>max</sub> <sup>b,c</sup> (%)
A	0.15,0.13	18,980	456	59	3.98/3.50/3.95	2.80/2.64/1.96	3.61/3.10/3.57
B	0.16,0.12	6140	448	60	1.32/1.32/1.20	1.14/0.89/0.53	1.33/1.30/1.27
p1	0.15,0.08	9902	444	52	3.5/3.15/2.36	2.59/2.04/1.03	4.68/4.40/3.35
p2	0.15,0.09	9539	444	52	3.2/3.08/2.41	2.51/2.10/1.11	3.92/3.92/3.09
m1	0.15,0.04	3748	436	51	1.2/0.92/–	0.95/0.53/–	2.81/2.26/–
m2	0.15,0.04	4091	436	51	1.2/0.90/–	0.93/0.52/–	2.84/2.24/–

<sup>a</sup> At 100 cd m<sup>-2</sup>.

<sup>b</sup> Maximum at 100 cd m<sup>-2</sup>.

<sup>c</sup> Maximum at 1000 cd m<sup>-2</sup>.

Electroluminescent characteristics of the doped devices are also shown in Table 2 and Fig. 6. From Fig. 6a, the maximum emission (λ<sub>max</sub>) of devices of p1, p2, m1 and m2 are located at 444, 444, 436 and 436 nm, and the full width at half-maximum (FWHM) values are 52, 52, 51 and 51 nm, respectively. The p-PABPI-doped devices p1 and p2 exhibited the maximum current efficiencies of 3.5 and 3.2 cd A<sup>-1</sup>, the maximum power efficiencies of 2.59 and 2.51 lm W<sup>-1</sup>, and the EQE of 4.68% and 3.92%, respectively. Notably, as dopant concentration of p-PABPI is increased from 3 wt% to 6 wt%, the integral performance of OLEDs declines to a certain extent, which is ascribed to the increase of dopant concentration for p-PABPI that may strengthen the response of concentration-quenching. The devices p1 and p2 showed pure blue emission with CIE coordinates of (0.15, 0.08) and (0.15, 0.09), which are close to the blue standards (0.14, 0.08) of NTSC. Curiously, a relatively rare blue-violet emission was found for the m-PABPI-doped devices with CIE coordinates (x, y) of (0.15, 0.04), which may owe to a low doping concentration to prevent red-shift and an effective host and guest energy level pairing that enables excitons to be generated on

the host to trigger short wavelength emission [32]. More importantly, prior to p-PABPI, the CIE<sub>x,y</sub> (0.15, 0.04) of m-PABPI-doped devices is independent to dopant concentration. The independence may be related to the more twisted molecular configuration that prevents close molecular stacking.

#### 4. Conclusions

Two novel twisted anthracene derivatives (p-PABPI and m-PABPI) were successfully designed and synthesized as blue emitters in OLEDs. The non-doped blue fluorescent organic light-emitting diodes were fabricated with the structure of ITO/MoO<sub>3</sub> (5 nm)/NPB (40 nm)/TCTA (5 nm)/EML: p-PABPI and m-PABPI (20 nm)/B<sub>3</sub>PyPB (40 nm)/LiF (1 nm)/Al (100 nm) by vacuum deposition. The devices with p-PABPI showed the efficiencies of 18,980 cd m<sup>-2</sup>, 3.98 cd A<sup>-1</sup>, 2.80 lm W<sup>-1</sup> as well as a blue emission with CIE coordinates of (0.15, 0.13) and little efficiency roll-off and color change at high brightness. It is particularly intriguing that the efficiencies of p-PABPI are almost three times larger than that of m-PABPI

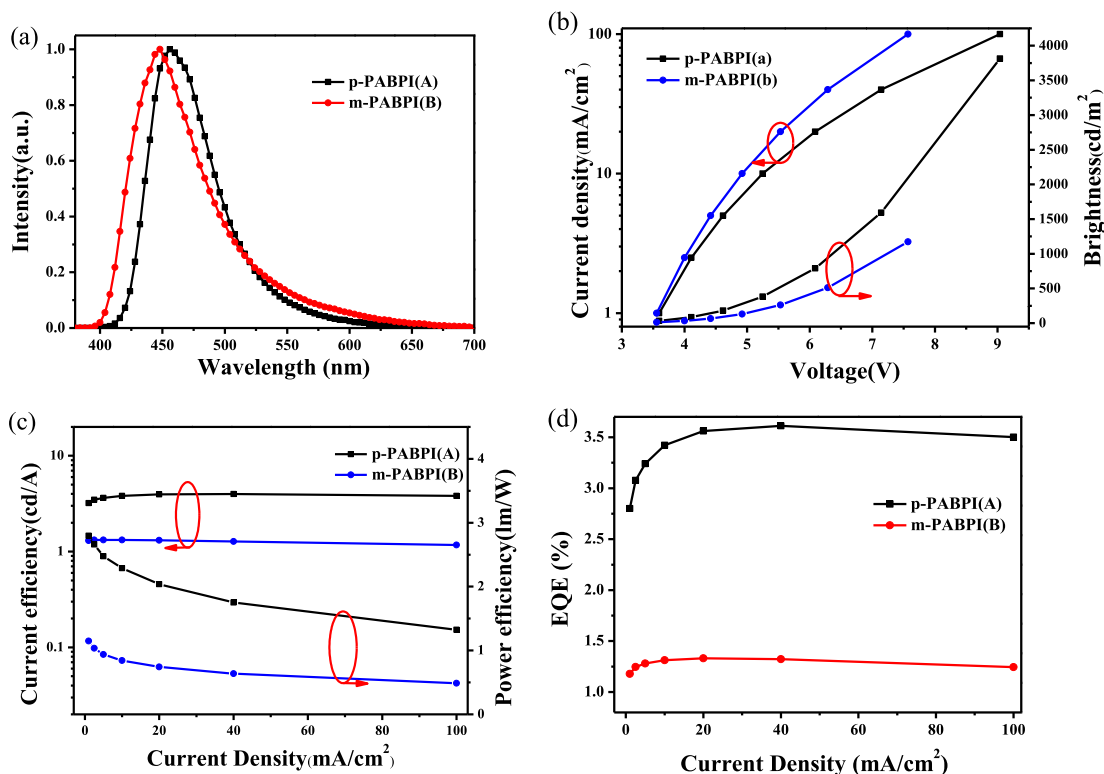


**Fig. 5.** Electroluminescent result of the non-doped devices: (a) EL spectra; (b) Current density-voltage-luminance characteristics curves; (c) Current efficiency curves and power efficiency curves versus current density; (d) The external quantum efficiency curves.

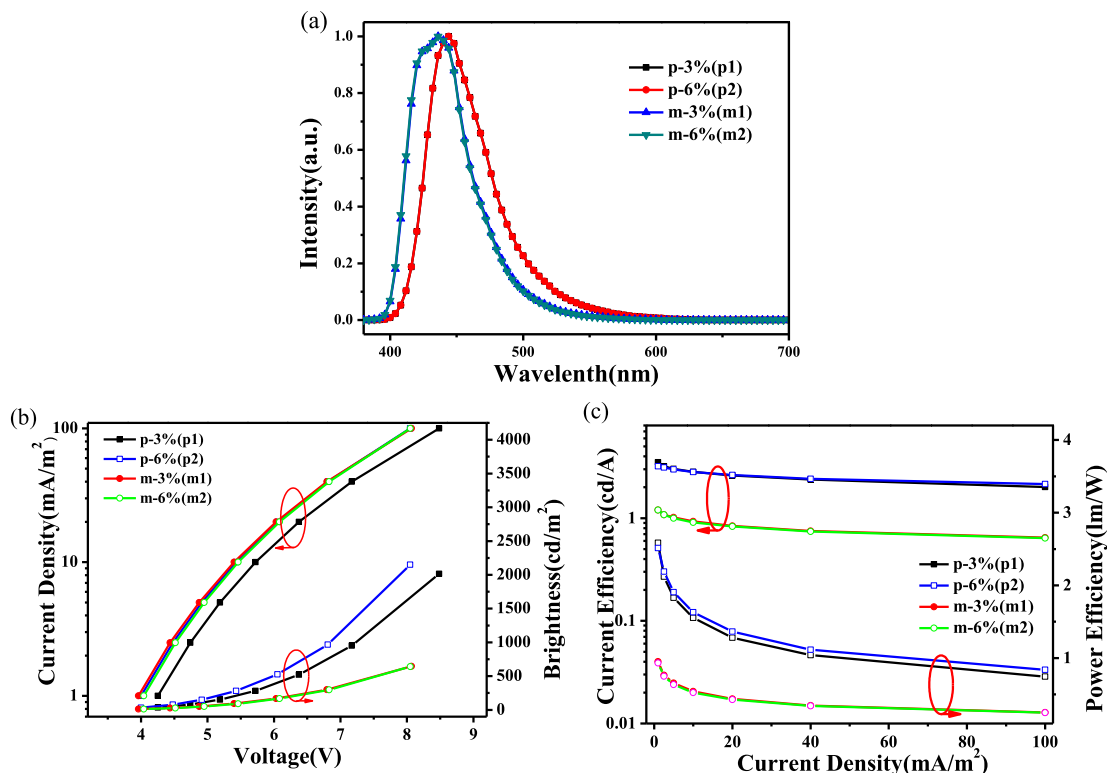


Fig. 6. Electroluminescent result of the doped devices: (a) EL spectra; (b) Current density-voltage-luminance characteristics curves; (c) Current efficiency curves and power efficiency curves versus current density.

through changing the constitution of phenyl between anthracene and imidazole. In addition, the doped OLED devices with the configuration of ITO/MoO<sub>3</sub> (5 nm)/NPB (40 nm)/TCTA (5 nm)/p-PABPI or m-PABPI: CBP (20 nm, 3 wt% or 6 wt%)/B<sub>3</sub>PyPB (40 nm)/LiF (1 nm)/Al (100 nm) were fabricated, where CBP was used as a host. The m-PABPI-doped devices showed a relatively rare blue-violet emission with CIE coordinate of (0.15, 0.04), which is independent to dopant concentration. The results provide a new approach of molecular design for obtaining high performance blue emission materials based on anthracene derivatives.

## Acknowledgments

This work was financially supported from the National Natural Science Foundation of China (51273209 and 514111004), the External Cooperation Program of the Chinese Academy of Sciences (No. GJHZ1219), Ningbo Natural Science Foundation (201401A6105063), and Open Research Fund of State Key Laboratory of Polymer Physics and Chemistry (201404), Changchun Institute Applied Laboratory of Polymer Physics and Chemistry, CAS. Ms J W is also thankful to Prof. Xinhua Ouyang (NIMTE) for analysis and discussion.

## Appendix A. Supplementary data

Supplementary data related to this article can be found at <http://dx.doi.org/10.1016/j.dyepig.2015.03.005>.

## References

- [1] Sasabe H, Kido J. Development of high performance OLEDs for general lighting. *J Mater Chem C* 2013;1:1699–707.
- [2] Chen C-H, Huang W-S, Lai M-Y, Tsao W-C, Lin JT, Wu Y-H, et al. Versatile, benzimidazole/amine-based ambipolar compounds for electroluminescent

- applications: single-layer, blue, fluorescent OLEDs, hosts for single-layer, phosphorescent OLEDs. *Adv Funct Mater* 2009;19:2661–70.
- [3] Zhang X, Lin J, Ouyang X, Liu Y, Liu X, Ge Z. Novel host materials based on phenanthroimidazole derivatives for highly efficient green phosphorescent OLEDs. *J Photochem Photobiol A Chem* 2013;268:37–43.
- [4] Zhu M, Yang C. Blue fluorescent emitters: design tactics and applications in organic light-emitting diodes. *Chem Soc Rev* 2013;42:4963–76.
- [5] Kim M-J, Lee C-W, Gong M-S. New spirobenzanthracene derivatives with naphthylanthracene core: synthesis and application in sky-blue fluorescent host materials. *Dyes Pigments* 2014;105:202–7.
- [6] Liang H, Wang X, Zhang X, Liu Z, Ge Z, Ouyang X, et al. Saturated deep-blue emitter based on a spiro[benzanthracene-fluorene]-linked phenanthrene derivative for non-doped organic light-emitting diodes. *New J Chem* 2014;38:4696–701.
- [7] Sasabe H, Gonmori E, Chiba T, Li Y-J, Tanaka D, Su S-J, et al. Wide-energy-gap electron-transport materials containing 3,5-dipyridylphenyl moieties for an ultra high efficiency blue organic light-emitting device. *Chem Mater* 2008;20:5951–3.
- [8] Su S-J, Gonmori E, Sasabe H, Kido J. Highly efficient organic blue-and white-light-emitting devices having a carrier- and exciton-confining structure for reduced efficiency roll-off. *Adv Mater* 2008;20:4189–94.
- [9] Xiao L, Su S-J, Agata Y, Lan H, Kido J. Nearly 100% internal quantum efficiency in an organic blue-light electrophosphorescent device using a weak electron transporting material with a wide energy gap. *Adv Mater* 2009;21:1271–4.
- [10] Dias FB, Bourdakos KN, Jankus V, Moss KC, Kamtekar KT, Bhalla V, et al. Triplet harvesting with 100% efficiency by way of thermally activated delayed fluorescence in charge transfer OLED emitters. *Adv Mater* 2013;25:3707–14.
- [11] Yook KS, Lee JY. Organic materials for deep blue phosphorescent organic light-emitting diodes. *Adv Mater* 2012;24:3169–90.
- [12] Pope M, Kallmann HP, Magnante P. Electroluminescence in organic crystals. *J Chem Phys* 1963;38:2042–3.
- [13] Koguchi N, Takahashi S. Double-heterostructure Pb<sub>1-x-y</sub>Cd<sub>x</sub>Sr<sub>y</sub>S/PbS/Pb<sub>1-x-y</sub>Cd<sub>x</sub>Sr<sub>y</sub>S lasers grown by molecular beam epitaxy. *Appl Phys Lett* 1991;58:799–800.
- [14] Lee M-T, Chen H-H, Liao C-H, Tsai C-H, Chen CH. Stable styrylamine-doped blue organic electroluminescent device based on 2-methyl-9,10-di(2-naphthyl)anthracene. *Appl Phys Lett* 2004;85:3301–3.
- [15] Huang JH, Su J-H, Li X, Lam M-K, Fung K-M, Fan H-H, et al. Bipolar anthracene derivatives containing hole- and electron-transporting moieties for highly efficient blue electroluminescence devices. *J Mater Chem* 2011;21:2957–64.
- [16] Zhuang S, Shangguan R, Huang H, Tu G, Wang L, Zhu X. Synthesis, characterization, physical properties, and blue electroluminescent device applications of phenanthroimidazole derivatives containing anthracene or pyrene moiety. *Dyes Pigments* 2014;101:93–102.

- [17] Zhang P, Dou W, Ju ZH, Yang LZ, Tang XL, Liu WS, et al. A 9,9'-bianthracene-core molecule enjoying twisted intramolecular charge transfer to enhance radiative-excitons generation for highly efficient deep-blue OLEDs. *Org Electron* 2013;14:915–25.
- [18] Li WJ, Liu DD, Shen FZ, Ma DG, Wang ZM, Feng T, et al. A twisting donor-acceptor molecule with an intercrossed excited state for highly efficient, deep-blue electroluminescence. *Adv Funct Mater* 2012;22:2797–803.
- [19] Ouyang X, Zhang X, Ge Z. Enhanced efficiency in nondoped, blue organic light-emitting diodes utilizing simultaneously local excitation and two charge-transfer exciton from benzimidazole-based donor–acceptor molecules. *Dyes Pigments* 2014;103:39–49.
- [20] Teng C, Yang X, Yang C, Li S, Cheng M, Hagfeldt A, et al. Molecular design of anthracene-bridged metal-free organic dyes for efficient dye-sensitized solar cells. *J Phys Chem C* 2010;114:9101–10.
- [21] Teki Y, Toichi T, Nakajima S.  $\pi$  topology and spin alignment in unique photoexcited triplet and quintet states arising from four unpaired electrons of an organic spin system. *Chem A Eur J* 2006;12:2329–36.
- [22] Zhang X, Xu Z, Ge Z, Ouyang X, Ji W. Tunable molecular configuration for significant enhancement of two-photon absorption based on novel octupolar benzoimidazole derivatives. *J Photochem Photobiol A Chem* 2014;290:22–30.
- [23] Liang HJ, Wang XX, Zhang XY, Ge ZY, Ouyang XH, Wang SD. Efficient tuning of electroluminescence from sky-blue to deep-blue by changing the constitution of spirobenzofluorene derivatives. *Dyes Pigments* 2014. <http://dx.doi.org/10.1016/j.dyepig.2014.04.019>.
- [24] Cho I, Kim SH, Kim JH, Parka S, Park SY. Highly efficient and stable deep-blue emitting anthracene-derived molecular glass for versatile types of non-doped OLED applications. *J Mater Chem* 2012;22:123–9.
- [25] Zhuang S, Shangguan R, Jin J, Tu G, Wang L, Chen J, et al. Efficient nondoped blue organic light-emitting diodes based on phenanthroimidazole-substituted anthracene derivatives. *Org Electron* 2012;13:3050–9.
- [26] Shin M-G, Kim SO, Park HT, Park SJ, Yu HS, Kim Y-H, et al. Synthesis and characterization of ortho-twisted asymmetric anthracene derivatives for blue organic light emitting diodes (OLEDs). *Dyes Pigments* 2012;92:1075–82.
- [27] Gong M-S, Lee H-S, Jeon Y-M. Highly efficient blue OLED based on 9-anthracene-spirobenzofluorene derivatives as host materials. *J Mater Chem* 2010;20:10735–46.
- [28] Chang Y-C, Yeh S-C, Chen Y-H, Chen C-T, Lee R-H, Jeng R-J. New carbazole-substituted anthracene derivatives based non-doped blue light-emitting devices with high brightness and efficiency. *Dyes Pigments* 2013;99:577–87.
- [29] Xing X, Zhong L, Zhang L, Chen Z, Qu B, Chen E, et al. Essential differences of organic films at the molecular level via vacuum deposition and solution processes for organic light-emitting diodes. *J Phys Chem C* 2013;117:25405–8.
- [30] Wang K, Wang S, Wei J, Chen S, Liu D, Liu Y, et al. New multifunctional phenanthroimidazole-phosphine oxide hybrids for high-performance red, green and blue electroluminescent devices. *J Mater Chem C* 2014;2:6817–26.
- [31] Hu J-Y, Pu Y-J, Satoh F, Kawata S, Katagiri H, Sasabe H, et al. Bisanthracene-based donor–acceptor-type light-emitting dopants: highly efficient deep-blue emission in organic light-emitting devices. *Adv Funct Mater* 2014;24:2064–71.
- [32] Jou J-H, Chen Y-L, Tseng J-R, Wu R-Z, Shyue J-J, Justin Thomas KR, et al. The use of a polarity matching and high-energy exciton generating host in fabricating efficient purplish-blue OLEDs from a sky-blue emitter. *J Mater Chem* 2012;22:15500–6.